Advanced Characterisation of Rammed Earth and Hemp Concrete: Towards Hybrid Solution

Sara Khalil[1], Omayma Homoro[1], Salah Ouldboukhitine[1], Sofiane Amziane[1]

[1] *Université Clermont Auvergne, Clermont Auvergne INP, CNRS, Institut Pascal, F-63000 Clermont–Ferrand, France*

RESUME Interest in using earth and bio-based materials for eco-friendly construction is increasing, with rammed earth (RE) and hemp concrete (HC) attracting considerable attention. While RE offers strong structural benefits, its insulation properties, especially in colder weather, are often insufficient. To address this, a hybrid double-layer wall is proposed, using RE as the core load-bearing layer and HC as the external insulation. The low density and porous structure of HC help limit heat transfer, improving energy efficiency. However, to ensure the feasibility and performance of this combination, a detailed assessment of the physical and mechanical properties of each material individually is necessary before their integration. Therefore, this study examines their fundamental characteristics and employs the Digital Image Correlation (DIC) technique to capture full-field displacement and strain, offering detailed insights into the materials behaviour. Understanding these aspects will guide the optimized design of the hybrid wall system, ultimately improving the overall performance of rammed earth constructions, while maintaining their environmental and structural advantages.

Mots-clefs rammed earth, hemp concrete, mechanical characterisation, DIC, hybrid insulation solution

I. Introduction

Earth materials have been used in construction for millennia, providing a sustainable and durable building solution. Among these, rammed earth (RE) construction is a traditional technique valued for its environmental benefits, offering high thermal mass, which enhances energy efficiency and indoor thermal comfort (Beckett, 2012; Maniatidis and Walker, 2003). Additionally, RE structures are durable, fire-resistant, and aesthetically appealing, seamlessly blending with their surroundings. Despite its labour-intensive process and need for skilled craftsmanship, RE construction is experiencing renewed interest due to its potential for sustainable and resilient building applications.

However, RE generally exhibits low mechanical resistance under uniaxial compression and direct tension (Maniatidis and Walker, 2003), and also lacks sufficient insulation – particularly in cold climates – necessitating the integration of insulation layers to meet modern thermal regulations. When adding insulation to RE wall, one of the main concerns is moisture-related damage. This can result from condensation within the wall, trapped water vapor due to the use of too-closed insulating materials, or the ingress of liquid water from external sources or capillary rise (Ple et al., 2024). If not properly managed, excessive water accumulation in rammed earth

material can lead to a deterioration in its mechanical resistance (Chauhan et al., 2019; Heitz et al., 2015; Morel et al., 2021) and can cause the material to fail. Insulation design must therefore guarantee a balanced water state to avoid any structural failure.

In rehabilitation projects and occupied buildings, external insulation is often the preferred solution, as it improves winter comfort while preserving the thermal mass properties of RE. Previous studies have demonstrated the effectiveness of external insulation, reporting acceptable indoor temperatures during winter and summer (Cheikhi et al., 2020; Serrano et al., 2016; Soebarto, 2009). While conventional insulation materials provide high thermal efficiency, their manufacturing processes are energy-intensive and environmentally taxing (Cetiner and Shea, 2018; Dickson and Pavía, 2021). Consequently, bio-based materials are gaining interest as sustainable alternatives, requiring less energy for production, emitting fewer greenhouse gases, and offering hygroscopic properties that improve indoor air quality by regulating humidity and temperature (Antunes et al., 2019; Cosentino et al., 2023; Lafond and Blanchet, 2020).

Among bio-based materials, plant-based concrete (also known as vegetal concrete) has emerged as a promising alternative, incorporating bio-aggregates into the mineral binders. These materials not only reduce embodied energy but also act as carbon sequestration agents, capturing and storing CO_2 throughout their lifecycle (Pittau et al., 2019). Projections indicate that bio-based construction materials could contribute to a 27% reduction in carbon emissions by 2050. In addition to their environmental benefits, plant-based aggregates have shown potential in enhancing mechanical performance, including improvements in compressive and tensile strength (Koutous and Hilali, 2021; Laborel-Preneron, 2017; Li et al., 2006; Zhou et al., 2017). However, this effect remains under debate, as some bio-aggregates may compromise compressive strength. For example, hemp shives, derived from hemp plant stems, are among the most widely used bio-aggregates in Europe (Amziane et al., 2017). When combined with clay, lime, or cement-based binders, vegetal concrete can be tailored to achieve various densities, making it suitable for applications ranging from lightweight insulation to structural reinforcement (Arufe et al., 2021).

Building on this context, the present study explores the behaviour of rammed earth and hemp concrete materials in the purpose of developing a hybrid system that enhances thermal insulation while maintaining structural integrity. To achieve this, the paper presents an individual characterization of each material, integrating 2D Digital Image Correlation (DIC) technique to assess deformation behaviour under loading conditions. The findings aim to support the implementation of RE-HC hybrid walls in double-layered panel systems, contributing to the advancement of sustainable construction practices highlighting the risks and challenges.

II. Materials and Methods

A. Materials

1. Soil

Not all soils are suitable for rammed earth construction, as the optimal soils are typically found in regions with long-standing rammed earth buildings that have demonstrated their durability over centuries (Soudani, 2016). The Auvergne-Rhône-Alpes (AURA) region in southeast France is a

prime example, notable for its rich heritage of historical rammed earth structures, many of which require renovation, alongside a growing number of modern rammed earth constructions. Given this context, the soil used in this study was sourced from Oytier village, located in the Isère department within the AURA region. The selection of this soil sample aims to reflect the local geotechnical characteristics while supporting both the preservation and development of rammed earth architecture in the region. Historically, inhabitants of this area have recognized the soil's suitability and its perfect adaption to rammed earth constructions (Zawistowski et al., 2020).

To assess its suitability, geotechnical characterization was performed, including particle size distribution (PSD) following (NF P94-057, 1992) and Atterberg limits (liquid limit (LL), plastic limit (PL) and plasticity index (PI)), determination according to (NF EN ISO 17892-12, 2018). The characterization results, including grain fractions categorized based on particle diameter as defined by Maniatidis and Walker, 2003, are summarized in Table 1. Additionally, **Erreur ! Source du renvoi introuvable.** presents the PSD curve, illustrating the cumulative passing percentages as a function of particle size.

Several recommendations exist for evaluating soil suitability for rammed earth construction. Among them, (Walker et al., 2005), as also reviewed by (Ciancio and Jaquin, 2011), provide guidelines that define the range of the grain size, as referenced in Table 1, to assess the compatibility of the soil for rammed earth applications.

Table 1. Grain size fractions and Atterberg limits

Reference	Gravel [%]	Sand [%]	Silt [%]	Clay [%]	LL [%]	PL [%]	PI [%]
This work	45.3	26.9	14.4	13.4	30.4	16.9	13.5
(Walker et al., 2005)	Sand+ Gravel: 45 – 80		10 – 30	5 – 20	/ - 45	/	2 - 30

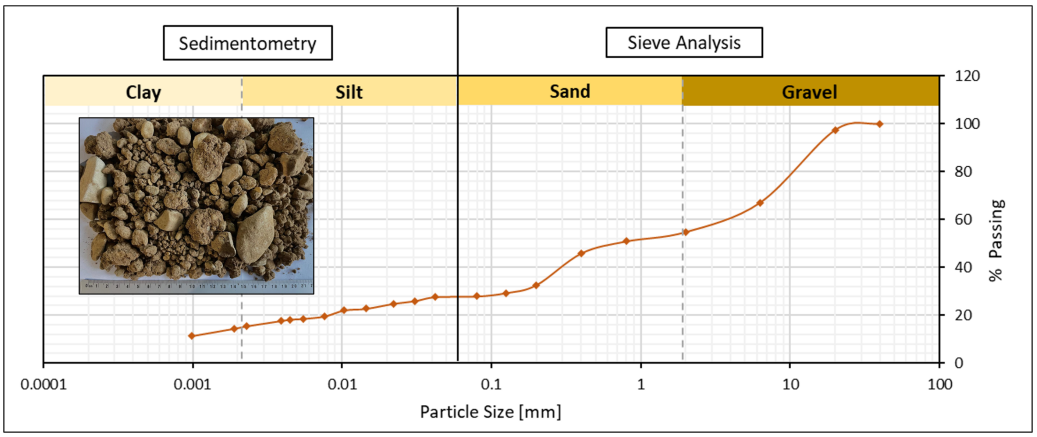

Figure 1. Particle size distribution curve

2. Bio-aggregates

The bio-aggregates used in this study are hemp shives (KANABAT), sourced from industrial hemp (Cannabis sativa) and supplied by "La Chanvière". According to the supplier, the hemp shiv particles range in size from 5 to 20 mm in length and 1 to 10 mm in width. Their composition is typically 52% cellulose, 9% hemicellulose, 18% lignin, 20% soluble, and 1% mineral matter.

The physical characterization of the hemp shives was conducted following the recommendations of the RILEM Technical Committee 236-BBM on bio-based materials (Amziane et al., 2017). As per these guidelines, the aggregates were dried at 60°C prior to testing until a constant mass was achieved, with a mass variation remaining below 0.1% over 24 hours.

- Bulk density:

The hemp shiv sample was placed in a cylindrical container measuring of 10 cm in diameter and 15 cm in height[1], with a material quantity adjusted to occupy half the volume of the container. The cylinder was then upending ten times. The volume was marked by a cardboard and measured with water. The test was repeated 3 times.

- Initial water content and water absorption rate:

The initial water content (W_0) of the hemp shives was determined using the equation: $W_0 = (M_0 – M_D)/ M_D \times 100$, where M_0 represents the initial mass of the aggregates (g), and M_D is the mass of the dry aggregates (g).

To assess water absorption, three dried samples of 25g each were placed in synthetic permeable bags and immersed in water. The mass gain was measured at 1 min, 15 min, 4 h, and 48 h. After each immersion period, the bags were placed in a salad spinner and wrung at 2 rotations per second for 60 seconds to remove superficial water. The water absorption capacity (W(t)) in % by weight was then calculated using the equation: W(t) = M(t) – MD / MD × 100, where M(t) is the mass of wet aggregates after each immersion time (g). Two other parameters are calculated being the initial rate of absorption (IRA) and K_1 that is associated with the rate of water diffusion within the hemp shiv cells and is closely linked to its intrinsic porosity based on the equation: $W(t) = IRA + K_1 \times \ln(t)$ (Bourdot et al., 2019).

The results, presented in Table 2, represent mean values obtained from three different samples, with a coefficient of variation (CV%) below 5%.

Table 2. Physical properties of the hemp shives.

Initial water content [%]		Bulk density [kg/m3]		Water absorption	
Average	CV%	Average	CV%	IRA %	K_1
11.6	1.025	88.8	2.84	146.53	19.037

3. Binders

Two mineral binders were used in this study: commercial lime (Tradical PF 70) and low-alkaline sulfoaluminate cement (CSA).

- Tradical PF 70 consists of 75% non-hydraulic lime (common lime), 15% hydraulic lime, and 10% pozzolan. The hydraulic lime and pozzolan contribute to the activation of carbonation, enhancing mechanical strength within a few days (Nguyen et al., 2009).
- CSA cement is composed of 81% clinker and 19% anhydrite, as reported in details by (Bardouh et al., 2024b)

[1] A container with a height at least twice its diameter is recommended, as suggested by (Amziane et al., 2017)

B. Mixing design and sample preparation

1. Rammed Earth (RE)

To simulate the compaction effort typically achieved through pneumatic placement in RE construction, a Proctor test was performed (NF P94-093, 2014). This test determines the optimum moisture content corresponding to the maximum dry density of the soil.

In collaboration with LOCIE Laboratory at "Université Savoie Mont-Blanc", this step was carried out by our partners, who recommended moisture content of approximately 11% for preparing the rammed earth specimens.

Three Cubic samples (15 × 15 × 15 cm^3) were fabricated, by compacting the wet soil in layers using a pneumatic rammer. First, an initial 10-11 cm layer was poured into the formwork and compacted at a pressure range of 6 – 6.5 bars, reducing its thickness to 5-6 cm. This process was repeated layer by layer until reaching the final volume (overall ~3 layers). The samples were then stored in a controlled environment around 20°C and 50% RH for eight weeks to allow mass stabilization prior to testing. Mass measurements were recorded weekly throughout this period.

2. Hemp Concrete (HC)

Similarly, cubic hemp concrete specimens (15 × 15 × 15 cm^3) were prepared using a binder:aggregate:water ratio of 1:0.5:1. Three HC specimens of each binder type, namely hemp-lime (HTrad) and hemp-cement (HCSA) concrete, were prepared and stored under controlled environmental conditions (20 ± 2°C, 50 ± 2% RH) for 5 to 6 months before testing. However, a 2-month period was sufficient to monitor the drying kinetics, with measurements taken once per week. Once the mass loss stabilized below 0.1%, the material was considered fully air-dried, and the corresponding drying time was recorded.

Table 2 presents the densities of the materials, categorized as follows:

- Initial density: The density measured immediately after de-molding.
- Stabilized density: The density at which the samples reached a constant weight after the drying period.
- Dry density: The density of specimens after oven-drying at 60°C over 48 hours, measured before testing.
- W_t [%]: Water content after equilibrium (by weight).

Table 3. Density values of rammed earth and hemp concrete specimens tested in this work

Samples	Mixture	Initial density [kg/m³]	Stabilized density [kg/m³]	Dry density [kg/m³]	W_t [%]
RE2	Oytier's raw earth	2026.3	1904.7	1856.4	2.6
RE3		2187.9	2014.9	1975.8	1.9
RE4		2248.3	2066.0	1985.9	4
Average		**2167.2 ±84**	**1995.2 ±67**	**1939.4 ±58**	**2.8 ±0.8**
HCSA-1	Hemp shives + CSA	518.5	376.3	340.2	10.6
HCSA-4		592.6	387.2	372.5	3.9
HCSA-5		592.6	391.5	384.9	1.7
Average		**567.9 ±34.9**	**376.3 ±18.5**	**365.9 ±18.8**	**5.4 ±3.7**

HTrad-1	Hemp shives + Tradical PF 70	526.9	434.1	398.9	8.8
HTrad-2		518.5	415.7	383.9	8.3
HTrad-3		548.2	424.3	388.8	9.1
Average		**543.2 ±18.5**	**424.7±7.5**	**390.5 ±6.2**	**8.7 ±0.3**

3. RE-HC Composite

In practice, a hemp concrete insulation panel—whether in dry-state (prefabricated panels) or wet state—will be externally applied to rammed earth, considering both renovation and new construction scenarios (Figure 2 (a)). Accordingly, several configurations need to be considered when combing the two materials.

This paper presents exclusively one configuration, in which both materials are used in wet state. It details the fabrication process, along with initial observations and challenges. This approach replicates the conditions of new construction, allowing the direct bonding between the materials.

Following the same mixing design and fabrication techniques described earlier, a 10 × 15× 20 cm^3 panels, for both RE and HC, were designed for the push-out test (**Erreur ! Source du renvoi introuvable.** (b)). The primary objective was to assess the mechanical performance of a double-layered RE-HC wall, specifically by evaluating the shear strength at the RE-HC interface.

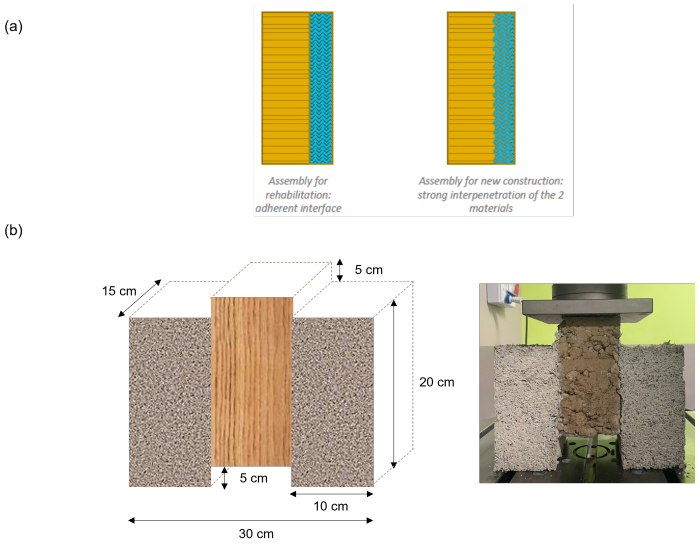

Figure 2. (a) Schematic representation of the double-layered assembly, (b) Push-out schematic low-scaled laboratory configuration and the tested sample

C. Test Setup

The compression tests were conducted using a Zwick Roell machine, with the load applied perpendicular to the compaction direction of the layers. For HC, three cycles of loading and unloading were applied between 1% and 3% deformation, with 1% increments per cycle, at loading and unloading velocities of 3 mm/min and 6 mm/min, respectively. Similarly, for rammed earth, three cycles were performed between 3 mm and 6 mm displacement, with 1.5 mm increments per cycle, maintaining the same loading and unloading velocities. The compression

test setup, in combination with the DIC technique, is illustrated in **Erreur ! Source du renvoi introuvable.** (a).

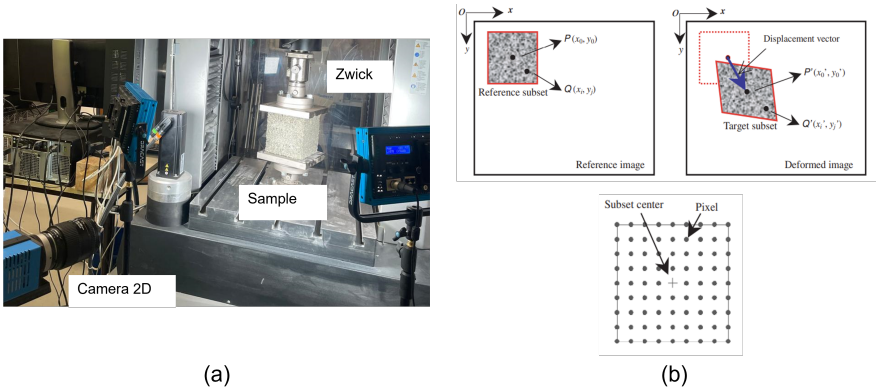

Figure 3. (a) Compression test setup and (b) the basic principle of subset-based DIC method (Pan et al., 2009)

A 2D Digital Image Correlation (DIC) technique was employed to analyse the displacement and deformation fields of the tested specimens. A PCO 2000 digital camera, equipped with a 2048 × 2048-pixel CCD sensor, was positioned in front of the specimen. Image acquisition was carried out using Camware64 software, capturing 1 image per second throughout the test duration.

Before processing the images, two key DIC parameters were defined: the subset size and step size, both set to 10 pixels. The fundamental principle of DIC involves tracking identical image points across sequential digital images of the specimen's surface, recorded before and after deformation (**Erreur ! Source du renvoi introuvable.** (b)). For a detailed explanation of the methodology, the procedure is comprehensively described by (Bardouh et al., 2024b).

D. Thermal conductivity

Thermal conductivity measurements were conducted on oven-dried samples using the hot-wire probe method, operated by NEOTIM. The hot-wire probe was positioned between two samples, ensuring optimal contact to minimize air gaps, which could affect measurement accuracy.

The device is capable of measuring thermal conductivity values ranging from 0.02 to 5 $W \cdot m^{-1} \cdot K^{-1}$, with an accuracy of ±5% and a reproducibility of ±3%. Further details on the procedure can be found in (Benkhaled, 2020).

III. Results and Discussion

A. Individual Characterization

Table 4 presents the average values of the investigated parameters, including dry density (ϱdry), thermal conductivity (λ), compressive strength (σc), compressive strength at 1.5% strain ($\sigma_{c,1.5\%}$) Young's modulus (E), and peak strain (εp). The Young's modulus was determined using the floating modulus method, as described by (Niyigena et al., 2016). The peak strain (εp) represents the deformation level at which the material reached its maximum stress.

Table 4. Average values of the physical and mechanical properties of the tested specimens

Properties		RE		HCSA		HTrad	
		Average	CV %	Average	CV %	Average	CV %
Physical	ϱ_{dry} [kg/m3]	1939.42	3.03	365.88	5.1	390.55	1.6
	λ [W.m^{-1}.K^{-1}]	1.283	6.3	0.056	-	0.06	1.38
Mechanical	σ_c (MPa)	2.088	5.7	0.32	7.9	0.59	8.9
	$\sigma_{c,1.5\%}$ (MPa)	0.2	18.9	0.128	8.8	0.146	11.07
	E (MPa)	97.92	24.9	20.94	32.48	28.57	27.6
	ε_p (mm/mm)	0.069	4.9	0.097	12.83	0.139	6.8

The thermal conductivity of HCSA and HTrad was approximately 95% lower than that of RE. This difference is primarily attributed to the denser structure of RE, resulting from the higher compaction energy applied during fabrication. Among the hemp concrete formulations, HCSA recorded the lowest thermal conductivity (0.056 W/m·K) and the lowest density (365.88 kg/m³), reinforcing the well-established correlation between density and thermal conductivity, as highlighted by (Ávila et al., 2021).

In terms of mechanical behaviour, HCSA and HTrad exhibited higher peak strain values, ranging between 8% and 12% for HCSA and between 12% and 15% for HTrad, whereas RE reached peak strain values between 6% and 7% which are relatively higher than those reported in the literature (values < 3%) (Ávila et al., 2023; Koutous and Hilali, 2023; Maniatidis and Walker, 2008). To facilitate material comparisons and maintain a strain level relevant to practical applications, a 1.5% strain threshold was adopted for compressive strength evaluation, following the recommendations of (Cerezo, 2005) for hemp concrete, later applied by several researchers.

It is also worth noting that the coefficient of variation (CV) exceeding 10%, suggesting the influence of several factors. In the case of rammed earth, variations may arise from uneven compaction between layers, slight volume change due to high compaction pressure that caused the framework to swell, and heterogeneous grain distribution within each compacted layer. For hemp concrete, the variability could be linked to differences in mix preparation, as the samples were fabricated in multiple batches, potentially leading to slight variations in the precision of the associated ratio. Despite these disparities, RE exhibited the highest compressive strength (~2 MPa) and Young's modulus (~100 MPa), highlighting its high rigidity while its stress at 1.5% strain (~0.2 MPa) accounts for only 10% of its maximum strength. This implies that the material does not develop significant strength at low strain levels, meaning it remains relatively unstressed until a higher strain threshold is reached. Unlike Ávila et al., 2023, where $\sigma_{c,1.5\%}$ was around 70% of its peak strength. In this case, it may be said that it is irrelevant to assess the $\sigma_{c,1.5\%}$ of RE as it still has a long way to go before reaching peak strength.

Among the HC formulations, HCSA reached the lower maximum compressive strength of ~0.32 MPa and a Young's modulus of ~21 MP. At 1.5% strain, it shows approximately 40% of its peak strength (~0.128 MPa), indicating a higher capacity for plastic deformation compared to RE. A similar trend was observed for HTrad, exhibiting a compressive strength ~0.6 MPa and Young's modulus ~30 MPa, outperforming HCSA in both strength and stiffness. At 1.5% strain, HTrad shows around 26% of its peak strength, which is slightly lower in relative terms compared to

HCSA. However, its higher absolute mechanical properties confirm its improved performance compared to HCSA.

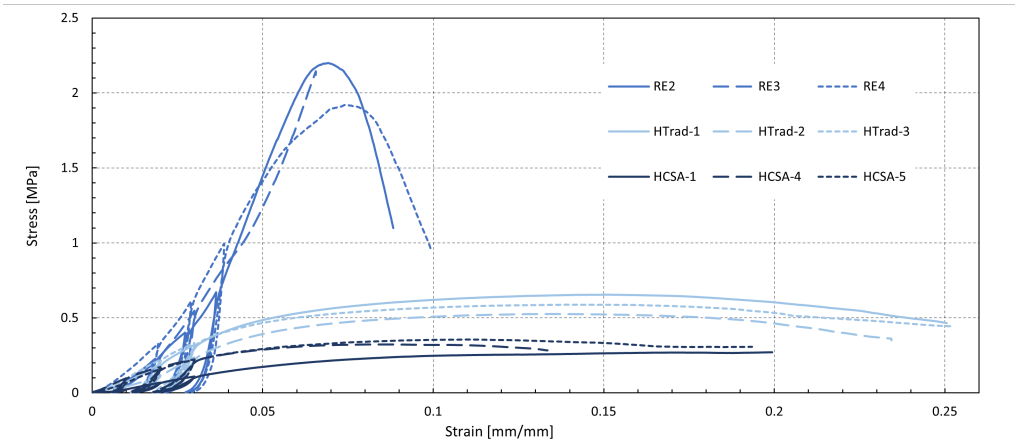

Figure 4. Stress-strain curves of the studied specimens

Figure 4 presents the strain-stress curves of the tested specimens. As shown, the mechanical behaviour of rammed earth exhibits a distinct two-phase response characterized by limited post-peak ductility. The material fails abruptly once its peak load-bearing capacity is reached. In contrasts, HC materials follows a three-phase mechanical response—quasi-elastic, elastoplastic, and gentle softening phases, as described by (Bardouh et al., 2024a). Unlike rammed earth—which transitions abruptly from an elastic phase, marked by very limited plastic deformation due to microcracking and grain rearrangement, to sudden brittle failure—hemp concrete exhibits a more gradual loss of strength, resulting in a plateau-like response after peak load.

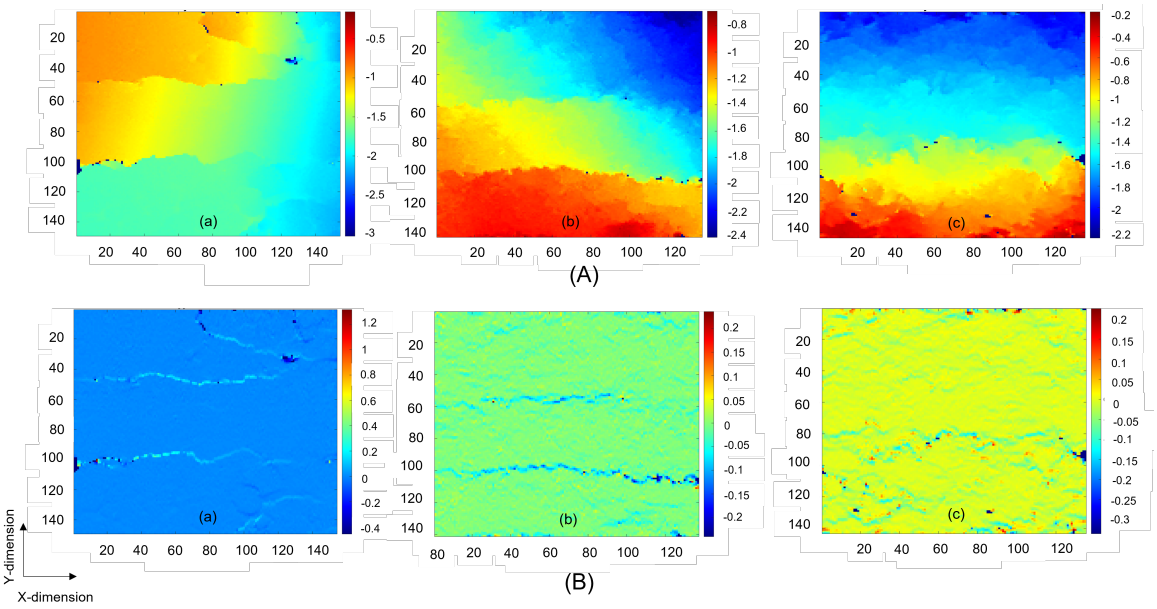

Figure 5. DIC outputs: (A) vertical full field displacement dy [mm] and (B) vertical strain εyy considering that for (a) RE4 at 5% strain rate, (b) HCSA-5 and (c) HTrad-1 at 1.5% strain rate

To further analyse the deformation behaviour of the materials, Figure 5 presents the vertical full field displacements d_y (A) and strains ε_{yy} (B) distribution over the entire surface of three selected specimens: (a) RE4, (b) HCSA-5, and (c) HTrad-1. For the RE sample, the presented fields correspond to load at a strain rate of 5% and the hemp concrete samples corresponds to that of 1.5%.

Overall, the d_y field for HSCA-5 and HTrad-1 exhibits a clear gradient, with the upper region displaying the highest displacement and the least displacement at the bottom part (Figure 5 (A, (b) and (c))). This suggests that the material deforms progressively from top to bottom, meaning that the upper layers experience more vertical movement under compression. The displacement distribution is relatively uniform for HTrad-1 and not HCSA-5, but the transition between regions is more pronounced, suggesting a higher degree of flexibility in comparison to rammed earth, where the behaviour of RE suggests that the material is undergoing homogeneous deformation, with no clear signs of localized failure yet (Figure 5 (A, (a))). However, minor strain concentration areas at the top indicate potential initiation of cracks (Figure 5 (B, (a))). The strain field appears mostly homogeneous, with a clear horizontal banding effect, indicating layered compaction behaviour from the fabrication process and the localized strain concentrations could be due to pre-existing weak zones between layers, where deformation concentrates. No widespread failure is observed, but the onset of cracking at these bands might indicate the beginning of structural degradation.

In contrast, the strain distribution in hemp concrete samples is more diffuse in HTrad-1, while in HCSA-5, the diffusion is less pronounced, with cracks appearing more distinctly at this phase. This difference may be attributed to uneven compaction efforts applied to HCSA samples during fabrication, which can lead to inconsistencies and localized stress concentrations. Both samples exhibit less sharply defined strain bands than rammed earth, confirming their more ductile behaviour (Figure 5 (B, (b) and (c)). And some localized strain concentrations are present but spread more evenly across the sample. But, for HTrad-1 sample, more scattered high-strain zones**,** suggesting slightly higher heterogeneity in deformation and that's depending on the binder type. Generally, in hemp concrete, bio-aggregates move without significantly deforming, with most of the strain concentrated within the binder matrix. As explained by (Amziane et al., 2024), this behaviour is associated with the interfacial transition zone (ITZ), where deformation occurs primarily in the binder surrounding the bio-aggregates, rather than the aggregates themselves. Their study highlights that damage in hemp concrete is often localized at binder-aggregate interfaces, leading to a diffuse failure mechanism across the material block, without direct mechanical contribution from the plant-based phase.

B. Hybrid solution: challenges and risks

The selected solution for combing rammed earth with hemp concrete was HTrad due to its better mechanical behaviour and sufficient thermal conductivity.

While preparing the RE-HC composite at the wet state we encountered significant challenges, particularly during the demoulding process. A total of four samples were prepared in this phase, each exhibiting distinct fabrication-related issues. Firstly, due to the fresh state of hemp concrete, the material exhibited low early-age cohesion, making it highly fragile and prone

to crumbling upon demoulding. To mitigate thus issue, the demoulding period was extended for some samples by keeping the composite within the formwork for over two weeks, allowing the HC panels to gain strength before demoulding. However, this led to a secondary issue—mould growth, as observed in Figure 6 (a, b). The extended confinement resulted in moisture retention and poor ventilation, creating favourable conditions for biological growth. This issue could be linked to water capillarity issues arise or in extremely humid climates (Giuffrida et al., 2024). Additionally, one of the samples demoulded immediately after fabrication exhibited detachment of the hemp concrete panel from the rammed earth core (Figure 6(c)). This separation suggests that the initial bond between RE and HC was weak, likely due to differential drying rates, shrinkage of the HC, or insufficient mechanical interlocking at the interface.

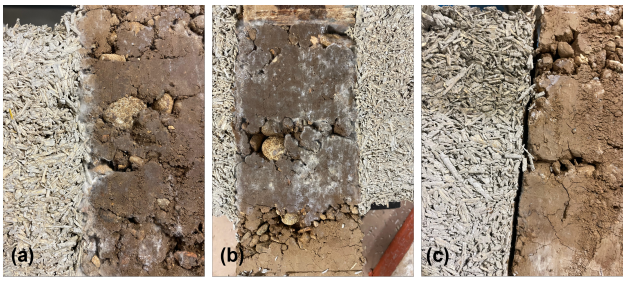

Figure 6. Issues encountered in the RE-HC configurations

As a result of these fabrication-related difficulties, only one of the prepared RE-HC composite specimens was successfully tested under the push-out configuration. As a result, the data obtained is not sufficient to be considered representative, and additional testing is required to confirm the shear behavior at the interface. Nonetheless, this preliminary result indicates a weak interfacial bond, suggesting that adhesion between the materials is limited in the current configuration. To address this, future work will focus on reinforcing the interface—particularly through the introduction of a binder layer—to enhance mechanical interlocking and improve shear resistance.

IV. Conclusion

This study investigated the mechanical and thermal properties of rammed earth and hemp concrete composites. Rammed earth exhibited high stiffness and strength but brittle failure, whereas hemp concrete showed lower mechanical performance but superior thermal insulation and ductility. Among the tested formulations, HTrad was selected as the optimal insulating layer, offering a balance between mechanical compatibility and thermal efficiency.

The fabrication process revealed several challenges, particularly in the wet-state integration of RE and HC. Issues such as early-age fragility of HC when demoulding, weak interface bonding, and mould growth due to prolonged curing underscored the complexities of combining these materials.

To overcome these challenges, optimized curing protocols, improved interface treatments, and refined mix designs are essential. Future research should focus on broader testing methods,

encompassing different scales to ensure the practical application and reliability of hybrid RE-HC systems in sustainable construction.

REFERENCES

Amziane, S., Collet, F., Lawrence, M., Magniont, C., Picandet, V., Sonebi, M., 2017. Recommendation of the RILEM TC 236-BBM: characterisation testing of hemp shiv to determine the initial water content, water absorption, dry density, particle size distribution and thermal conductivity. Mater. Struct. 50, 167. https://doi.org/10.1617/s11527-017-1029-3

Amziane, S., Toussaint, E., Collet, F., 2024. RILEM TC-275 (HDB): Presentation of TC HDB and mechanical performances of hemp concrete of the specimen of the round robin test. https://doi.org/10.21203/rs.3.rs-4425459/v1

Antunes, A., Faria, P., Silva, V., Brás, A., 2019. Rice husk-earth based composites: A novel bio-based panel for buildings refurbishment. Constr. Build. Mater. 221, 99–108. https://doi.org/10.1016/j.conbuildmat.2019.06.074

Arufe, S., Hellouin de Menibus, A., Leblanc, N., Lenormand, H., 2021. Effect of retting on hemp shiv physicochemical properties. Ind. Crops Prod. 171, 113911. https://doi.org/10.1016/j.indcrop.2021.113911

Ávila, F., Fagone, M., Gallego, R., Puertas, E., Ranocchiai, G., 2023. Experimental and numerical evaluation of the compressive and shear behavior of unstabilized rammed earth. Mater. Struct. 56, 118. https://doi.org/10.1617/s11527-023-02206-9

Ávila, F., Puertas, E., Gallego, R., 2021. Characterization of the mechanical and physical properties of unstabilized rammed earth: A review. Constr. Build. Mater. 270, 121435. https://doi.org/10.1016/j.conbuildmat.2020.121435

Bardouh, R., Toussaint, E., Amziane, S., Marceau, S., 2024a. Mechanical behavior of bio-based concrete under various loadings and factors affecting its mechanical properties at the composite scale: A state-of-the-art review. Clean. Eng. Technol. 23, 100819. https://doi.org/10.1016/j.clet.2024.100819

Bardouh, R., Toussaint, E., Amziane, S., Marceau, S., Berger Cokely, A.L., 2024b. Study of the mechanical behavior of hemp concrete with two different mineral binders through digital image correlation in various aggregate orientations, in: RILEM Conference on Sustainable Materials & Structures: Meeting the Major Challenges of the 21st Century - SMS 2024. Toulouse, France.

Beckett, C., 2012. A Review of the Contribution of Thermal Mass to Thermal Comfort in Rammed Earth Structures.

Benkhaled, M., 2020. Modélisation théorique et expérimentale du comportement énergétique et environnemental des matériaux de construction biosourcés (These de doctorat). Université Clermont Auvergne (2017-2020).

Bourdot, A., Magniont, C., Lagouin, M., Niyigena, C., Evon, P., Amziane, S., 2019. Impact of Bio-Aggregates Properties on the Chemical Interactions with Mineral Binder, Application to Vegetal Concrete. J. Adv. Concr. Technol. 17, 542–558. https://doi.org/10.3151/jact.17.542

Cerezo, V., 2005. Propriétés mécaniques, thermiques et acoustiques d'un matériau à base de particules végétales : approche expérimentale et modélisation théorique.

Cetiner, I., Shea, A.D., 2018. Wood waste as an alternative thermal insulation for buildings. Energy Build. 168, 374–384. https://doi.org/10.1016/j.enbuild.2018.03.019

Chauhan, P., El Hajjar, A., Prime, N., Plé, O., 2019. Unsaturated behavior of rammed earth: Experimentation towards numerical modelling. Constr. Build. Mater. 227, 116646. https://doi.org/10.1016/j.conbuildmat.2019.08.027

Cheikhi, W., Baba, K., Nounah, A., Cherradi, C., 2020. Effect of adding insulation on the energy performances of rammed earth buildings in hot and arid climates. E3S Web Conf. 150, 01011. https://doi.org/10.1051/e3sconf/202015001011

Ciancio, D., Jaquin, P., 2011. An Overview of Some Current Recommendations on the Suitability of Soils for Rammed Earth.

Cosentino, L., Fernandes, J., Mateus, R., 2023. A Review of Natural Bio-Based Insulation Materials. Energies 16, 4676. https://doi.org/10.3390/en16124676

Dickson, T., Pavía, S., 2021. Energy performance, environmental impact and cost of a range of insulation materials. Renew. Sustain. Energy Rev. 140, 110752. https://doi.org/10.1016/j.rser.2021.110752

Giuffrida, G., Ibos, L., Boudenne, A., Allam, H., 2024. Exploring the integration of bio-based thermal insulations in compressed earth blocks walls. Constr. Build. Mater. 418, 135412. https://doi.org/10.1016/j.conbuildmat.2024.135412

Heitz, P., Morel, J.-C., Fabbri, A., Soudani, L., Champiré, F., Meunier, N., 2015. Construction Terre L'isolation du Pisé : Pertinence et Principes. https://doi.org/10.13140/RG.2.1.1238.1688

Koutous, A., Hilali, E., 2023. Compression stress-strain curve of rammed earth: Measuring and modelling. Results Eng. 18, 101012. https://doi.org/10.1016/j.rineng.2023.101012

Koutous, A., Hilali, E., 2021. Reinforcing rammed earth with plant fibers: A case study. Case Stud. Constr. Mater. 14, e00514. https://doi.org/10.1016/j.cscm.2021.e00514

Laborel-Preneron, A., 2017. Formulation and characterization of unfired clay bricks with plant aggregates (phdthesis). Université Paul Sabatier - Toulouse III.

Lafond, C., Blanchet, P., 2020. Technical Performance Overview of Bio-Based Insulation Materials Compared to Expanded Polystyrene. Buildings 10, 81. https://doi.org/10.3390/buildings10050081

Li, Z., Wang, X., Wang, L., 2006. Properties of hemp fibre reinforced concrete composites. Compos. Part Appl. Sci. Manuf. 37, 497–505. https://doi.org/10.1016/j.compositesa.2005.01.032

Maniatidis, V., Walker, P., 2008. Structural Capacity of Rammed Earth in Compression. J. Mater. Civ. Eng. 20, 230–238. https://doi.org/10.1061/(ASCE)0899-1561(2008)20:3(230)

Maniatidis, V., Walker, P., 2003. A Review of Rammed Earth Construction: DTI Project Report.

Morel, J.-C., Charef, R., Hamard, E., Fabbri, A., Beckett, C., Bui, Q.-B., 2021. Earth as construction material in the circular economy context: practitioner perspectives on barriers to overcome. Philos. Trans. R. Soc. B Biol. Sci. 376, 20200182. https://doi.org/10.1098/rstb.2020.0182

NF EN ISO 17892-12, 2018. Reconnaissance et essais géotechniques - Essais de laboratoire sur les sols - Partie 12 : détermination des limites de liquidité et de plasticité.

NF P94-057, 1992. Sols : reconnaissance et essais - Analyse granulométrique des sols - Méthode par sédimentation.

NF P94-093, 2014. Sols : reconnaissance et essais - Détermination des références de compactage d'un matériau - Essai Proctor Normal - Essai Proctor modifié.

Nguyen, T.-T., Picandet, V., Amziane, S., Baley, C., 2009. Influence of compactness and hemp hurd characteristics on the mechanical properties of lime and hemp concrete. Eur. J. Environ. Civ. Eng. 13, 1039–1050. https://doi.org/10.1080/19648189.2009.9693171

Niyigena, C., Amziane, S., Chateauneuf, A., Arnaud, L., Bessette, L., Collet, F., Lanos, C., Escadeillas, G., Lawrence, M., Magniont, C., Marceau, S., Pavia, S., Peter, U., Picandet, V., Sonebi, M., Walker, P., 2016. Variability of the mechanical properties of hemp concrete. Mater. Today Commun. 7, 122–133. https://doi.org/10.1016/j.mtcomm.2016.03.003

Ple, O., Girerd, M., Prime, N., 2024. Analyse bibliographique préliminaire à l'étude du Comportement multifonctionnel de PArois Complexes géo et bio-Sourcées (ANR PACS+), in: Academic Journal of Civil Engenieering. Le Havres, France, pp. 229–239.

Serrano, S., de Gracia, A., Cabeza, L.F., 2016. Adaptation of rammed earth to modern construction systems: Comparative study of thermal behavior under summer conditions. Appl. Energy 175, 180–188. https://doi.org/10.1016/j.apenergy.2016.05.010

Soebarto, V., 2009. Analysis of Indoor Performance of Houses Using Rammed Earth Walls.

Soudani, L., 2016. Modelling and experimental validation of the hygrothermal performances of earth as a building material (These de doctorat). Lyon.

Walker, P., Keable, R., Martin, J., Architects, J., Maniatidis, V., 2005. Rammed earth: design and construction guidelines.

Zawistowski, K., Zawistowski, M., Joffroy, T., 2020. Evolving Vernacular: Reinventing Rammed Earth in the Context of Twenty-First Century Seismic Regulation. Technol. Des. 4, 158–165. https://doi.org/10.1080/24751448.2020.1804758

Zhou, X., Saini, H., Kastiukas, G., 2017. Engineering Properties of Treated Natural Hemp Fiber-Reinforced Concrete. Front. Built Environ. 3. https://doi.org/10.3389/fbuil.2017.00033